Supplementary Material (ESI) for Chemical Communications

Electronic Supplementary Information

Raman and computational study of solvation and chemisorption of thiazole in silver hydrosol

Maurizio Muniz-Miranda,*[a] Marco Pagliai,[a] Francesco Muniz-Miranda[b] and Vincenzo Schettino[a,b]

Experimental Details

Following the procedure proposed by Creighton et al.[1] the Ag hydrosols have been prepared by adding $AgNO_3$ (99.9999% purity, Aldrich) to excess $NaBH_4$ (99.9% purity, Aldrich). The ligand adsorption was obtained by adding thiazole (99% purity, Aldrich) to silver colloids in 10^{-3} M concentration. NaCl (99.998% purity, Aldrich) was added to Ag colloids in 10^{-3} M concentration to improve the SERS enhancement.

Raman spectra of thiazole as pure liquid, in CCl_4, in H_2O, in D_2O, in solution and in Ag hydrosol were recorded using the 514.5 nm line of a Coherent argon ion laser, a Jobin-Yvon HG2S monochromator equipped with a cooled RCA-C31034A photomultiplier, and a data acquisition facility. In the $400 - 1500\,cm^{-1}$ region the Raman spectrum of liquid thiazole closely corresponds, regarding frequencies and relative intensities, to that in CCl_4 solution. To impair the thermal effects due to the laser light, a defocused beam with low power (20 mW) was used. Power density measurements were performed with a power meter instrument (model 362; Scientech, Boulder, CO) giving ∼5% accuracy in the 300-1000 nm spectral range.

Computational Details

Car-Parrinello molecular dynamics simulation

Ab initio molecular dynamics simulation have been performed with the CPMD package[2] on a system made up of 64 heavy water and 1 thiazole molecules in the NVE ensemble. The sample has been simulated in a cubic box of edge length 12.6983 Å, with periodic boundary conditions. BLYP exchange and correlation functional[3,4] has been adopted, along with norm-conserving Martins-Troullier pseudopotentials[5] and Kleinman-Bylander decomposition.[6] Plane wave expansions have been truncated at 85 Ry while a 600 atomic units (a.u.) electronic fictitious mass has been set. The system has been simulated for about 26 ps with a time step of 4 a.u. (~ 0.096 fs). The average temperature was 302 ± 16 K.

Wavelet transform

Fourier Transform is usually employed to extract the frequency content from a time-dependent signal, without a simultaneous localization in both frequency and time domain. In order to obtain vibrational properties from molecular dynamics trajectories, Fourier Trasforms are performed,[7–9] but it has been recently shown[10–12] that similar results can be obtained with a wavelet analysis[13] approach.

Given an input function $f(t)$, its wavelet transform, $\mathcal{W}_n(s)$, is defined as

$$\mathcal{W}_n(s) = \int_{-\infty}^{+\infty} \mathrm{d}t'\, f(t')\psi^*\left(\frac{t'-n}{s}\right) \quad , \tag{1}$$

whose discretized expression is

$$\mathcal{W}_n(s) = \sum_{n'=0}^{N-1} f(n'\cdot\delta t)\psi^*\left(\frac{(n'-n)\cdot\delta t}{s}\right) \quad . \tag{2}$$

In the two previous equations, following the formalism of Torrence and Compo,[14], the ψ function is called "mother wavelet" and is stretched and translated in time by the two parameters s and n, respectively. n' is the time-step index, δt is the time step, s is the wavelet scale. The algorithm adopted for the present paper computed the wavelet transform in the Fourier space as:

$$\mathcal{W}_n(s) = \sum_{k=0}^{N-1} \hat{f}_k \cdot \hat{\psi}^*(s\omega_k) e^{i\omega_k n\delta t} \quad , \tag{3}$$

where k is the frequency index, ω_k is the angular frequency and $\hat{f}_k$ and $\hat{\psi}$ are the Fourier transforms of the time series f_n and of the mother wavelet ψ adopted, respectively. The mother wavelet used in this work is given by the Morlet function, since Kirby[15] proved it best reproduces the Fourier power spectrum:

$$\psi(t) = \pi^{-1/4} e^{i\omega_0 t - t^2/2\sigma^2}. \tag{4}$$

[a] *Dipartimento di Chimica "Ugo Schiff", via della Lastruccia 3, Sesto Fiorentino (FI), Italy. Fax: +390554573077; Tel: +390554573091; E-mail: muniz@unifi.it*

[b] *European Laboratory for Non-Linear Spectroscopy (LENS), via Nello Carrara 1, Sesto Fiorentino (FI), Italy.*

The ω_0 parameter has been set at 2π and with this choice the Fourier frequency is simply $\omega \simeq 1.01/s$.[14] The σ parameter affects the time-frequency resolution, which is governed by an uncertainty principle,[13] and has been put equal to 2 (as suggested by Mallik *et al.*[10,11]) in the analysis of *ab initio* molecular dynamics trajectories to allow a better time-frequency localization.

In Fig. S 1 a comparison between Fourier and wavelet trasforms of a test signal (a panel) is reported.

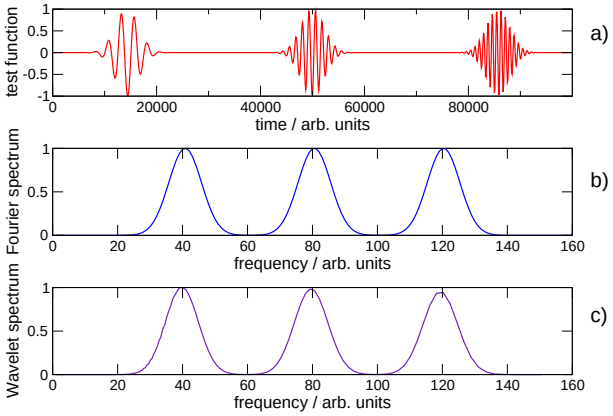

Fig. S 1 a) the test function defined in Eq. 5; b) its Fourier power spectrum; c) its wavelet spectrogram projected on the frequency axis (wavelet power spectrum). A value of 16 for the σ parameter has been adopted for a better frequency localization.

The test function is a cosine oscillating at three frequencies, modulated by Gaussian windows:

$$\begin{aligned} f(t) = &\cos(3\omega t)e^{-(t-t_3)^2/\tau} + \\ &\cos(2\omega t)e^{-(t-t_2)^2/\tau} + \\ &\cos(\omega t)e^{-(t-t_1)^2/\tau} \quad , \end{aligned} \tag{5}$$

with $\tau = 10^4$, $\omega = 0.0025$ and $t_3 > t_2 > t_1$. The Fourier power spectrum and the wavelet spectrogram projected on the frequency axis (wavelet power spectrum) of $f(t)$ are reported in panel b and c of Fig. S 1, respectively. The wavelet transforms not only are able to reproduce with good accuracy the Fourier power spectrum, but they also give spectrograms like the one in Fig. S 2, localizing the test signal both in time and frequency. Wavelet transform has been used to analyze the variation of the O-D bond length of the water molecule H-bonded to thiazole and a scaling factor of 1.05 has been adopted for the frequencies calculated from CPMD trajectories for a better agreement with the experimental Raman spectra as shown in Fig. S 3.

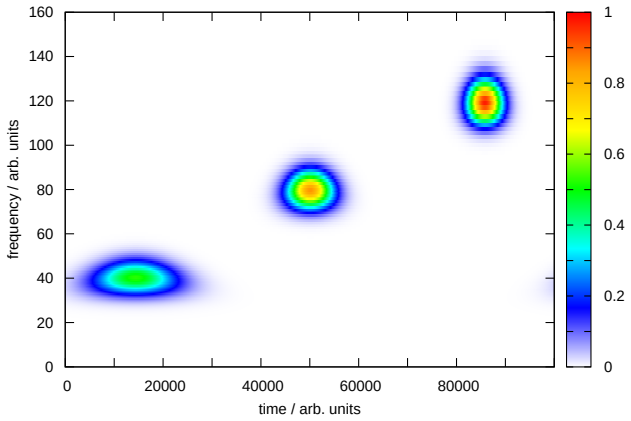

Fig. S 2 Wavelet spectrogram of the test function defined in Eq. 5. A value of 1 for the σ parameter has been adopted for a better time localization.

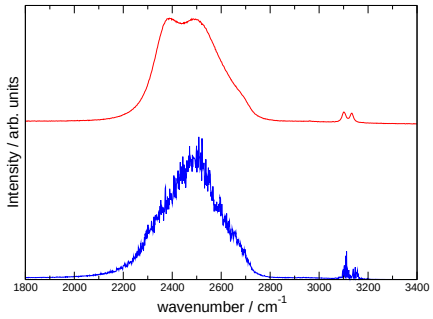

Fig. S 3 Comparison of experimental Raman spectrum of thiazole in D_2O (red upper line) with vibrational density of states (lower blue line) calculated by Fourier Transform of the velocity autocorrelation function (obtained by the CPMD simulation) corrected by a uniform scaling factor of 1.05.

Hydrogen bond function, F_{HB}

The F_{HB} function adopted is constructed as reported in Ref. 16

$$F_{HB} = A(r(t)) \cdot B(\theta(t)) \quad , \tag{6}$$

with $A(r(t))$ and $B(\theta(t))$ functions defined as

$$A(r(t)) = \begin{cases} \exp(-(r_e - r(t))^2/2\sigma_r^2) & \text{if } (r_e - r(t)) < 0, \\ 1 & \text{if } (r_e - r(t)) \geq 0; \end{cases}$$

$$B(\theta(t)) = \begin{cases} \exp(-(\theta_e - \theta(t))^2/2\sigma_\theta^2) & \text{if } (\theta_e - \theta(t)) < 0, \\ 1 & \text{if } (\theta_e - \theta(t)) \geq 0. \end{cases}$$

The values of the r_e, θ_e, σ_r and σ_θ parameters are taken from pair radial and angular unnormalized distribution functions $h(r)$ and $h(\theta)$ reported in Fig. S 4 b and d. Instead, in Fig. S 4 a and

c are reported the pair radial and angular distribution functions $g(r)$ and $g(\theta)$, along with the integration number, $n(r)$. r_e is the distance associated to the first local maximum in $h(r)$ and θ_e is the angle associated to the first local maximum of $h(\theta)$, whereas σ_r and σ_θ are the half-widths at half-height in $h(r)$ and $h(\theta)$, respectively.

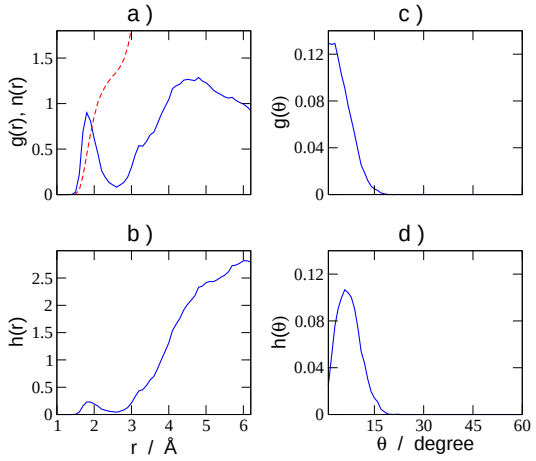

Fig. S 4 (*blue lines*) $g(r)$, $h(r)$, $g(\theta)$, $h(\theta)$, (*red line*) $n(r)$ for the N$\cdots$D interactions; r is the N$\cdots$D distance whereas θ is the N$\cdots$D $-$ O angle.

Raman and SERS spectra calculations

Raman and SERS spectra have been obtained by means of density functional calculations adopting the Gaussian 03 suite of programs.[17] B3LYP and BLYP functionals with 6-311++G(d,p) have been employed to check the effect of the functional on the calculated spectra, whereas the effect of the basis set has been tested with both 6-31+G(d,p) and 6-311++G(d,p). In all calculations the LANL2DZ basis set have been always adopted to describe the Ag atomic species. Geometries optimization and harmonic frequencies calculations have been performed with a very tight convergence criterion with an improved grid for the integral calculation, INTEGRAL(GRID=199974). The optimized geometries correspond to true energy minima, as revealed by the lack of imaginary values in the calculation of the vibrational modes. The calculated Raman activities (A_i) have been converted to relative Raman intensities (I_i) using the following relationship derived from the basic theory of Raman scattering:

$$I_i = f(\nu_0 - \nu_i)^4 \frac{A_i}{\nu_i} \left[1 - e^{-hc\nu_i/kT}\right] \quad , \qquad (7)$$

where ν_0 is the exciting frequency (in cm^{-1} units), ν_i is the vibrational frequency (in cm^{-1} units) of the i-th normal mode, h, c, and k are fundamental constants, and f is a suitably chosen common normalization factor for all peak intensities.

The calculated spectra were reported by assigning to each normal mode a Lorentzian shape with a 5 cm^{-1} full width at half-maximum.

The assignment of the Raman and SERS bands at B3LYP/6-311++G(d,p) level is reported in Table S 1, while the simulated Raman and SERS spectra at B3LYP/6-31+G(d,p) and BLYP/6-311++G(d,p) level of theory are reported in Fig. S5 and Fig. S6, respectively.

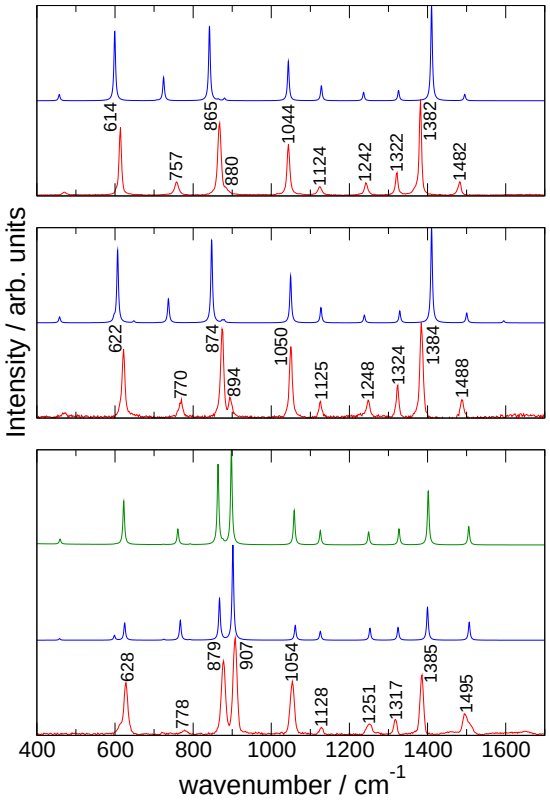

Fig. S 5 Raman spectra of thiazole in liquid (upper panel), aqueous solution (middle panel) and Ag hydrosol (lower panel) with observed frequencies (red line), compared with the DFT simulated spectra (blue line). In the SERS panel the green line is related to the thiazole/Ag_3^+ model, the blue line to thiazole/Ag^+ model. The calculations have been performed at B3LYP/6-31+G(d,p) level. Lanl2DZ basis set has been employed for silver.

liquid				aqueous solution		silver colloid		
exp.	calc.	symm.	assignment	exp.	calc.	exp.	calc. (Ag^+)	calc. (Ag_3^+)
	461	A''	ring torsion		460		460	461
614	601	A'	C-S symmetric stretch.	622	609	628	628	626
	602	A''	ring torsion		602	∼610	604	607
	714	A''	H wagging		716		729	728
757	724	A'	C-S asymmetric stretch.	770	736	778	767	761
	785	A''	H wagging		791		796	796
865	844	A'	ring bending	874	849	879	869	865
	869	A'	ring bending		880		882	883
880	885	A''	H wagging	894	883	907	909	905
1044	1045	A'	ring breathing	1050	1050	1054	1062	1059
1124	1129	A'	in plane H bending	1125	1128	1128	1128	1127
1242	1237	A'	in plane H bending	1248	1240	1251	1257	1252
1332	1325	A'	in plane H bending	1324	1328	1317	1321	1324
1382	1406	A'	(C=C,C=N) symmetric stretching	1384	1405	1385	1397	1398
1482	1495	A'	(C=C,C=N) asymmetric stretching	1488	1500	1495	1507	1506

Tab. S 1 Calculated and observed frequencies for thiazole liquid and for thiazole in water and in Ag colloid at B3LYP/6-311++G(d,p) level. Lanl2DZ basis set has been employed for silver. The calculated frequencies have been scaled for a 0.98 factor.

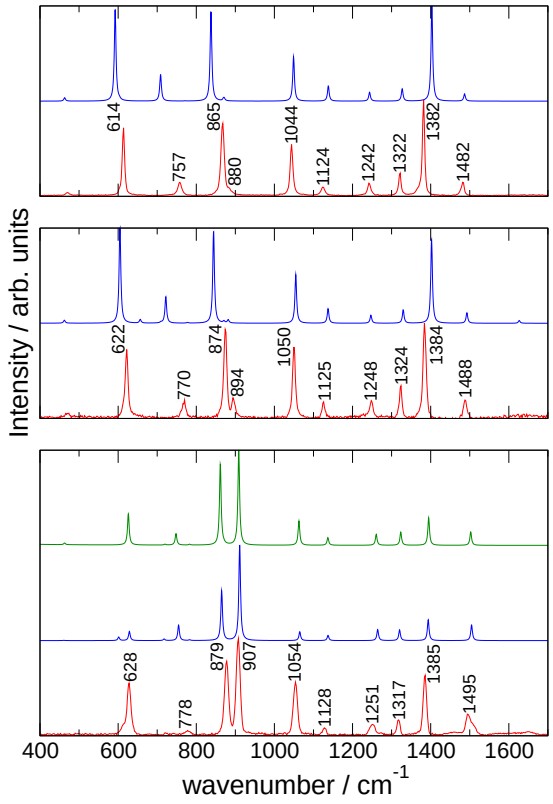

Fig. S 6 Raman spectra of thiazole in liquid (upper panel), acqueous solution (mittel panel) and Ag hydrosol (lower panel) with observed frequencies (red line), compared with the DFT simulated spectra (blue line). In the SERS panel the green line is related to the thiazole / Ag_3^+ model, the blue line to thiazole/Ag^+ model. The calculations have been performed at BLYP/6-311++G(d,p) level. Lanl2DZ basis set has been employed for silver.

References

1 J. A. Creighton, C. G. Blatchford and M. G. Albrecht, *J. Chem. Soc. Faraday Trans. II*, 1979, **75**, 790–798.

2 CPMD, *Copyright MPI für Festkörperforschung Stuttgart 1997-2001, Copyright IBM Corp 1990-2008*.

3 A. D. Becke, *Phys. Rev. A*, 1988, **38**, 3098–3100.

4 C. Lee, W. Yang and R. G. Parr, *Phys. Rev. B*, 1988, **37**, 785–789.

5 N. Troullier and J. L. Martins, *Phys. Rev. B*, 1991, **43**, 1993–2006.

6 L. Kleinman and D. M. Bylander, *Phys. Rev. Lett.*, 1982, **48**, 1425–1428.

7 M. E. Tuckerman, *Statistical Mechanics: Theory and Molecular Simulation*, Oxford University Press Inc., 2010.

8 B. J. Berne and R. J. Pecora, *Dynamic Light Scattering*, John Wiley and Sons Ltd., 1976.

9 D. A. McQuarrie, *Statistical Mechanics*, University Science Books, 2nd edn, 2000.

10 B. S. Mallik, A. Semparithi and A. Chandra, *J. Chem. Phys.*, 2008, **129**, 194512–194527.

11 B. S. Mallik, A. Semparithi and A. Chandra, *J. Phys. Chem. A*, 2008, **112**, 5104–5112.

12 A. Rahaman and R. Wheeler, *J. Chem. Theory Comput.*, 2005, **1**, 769–771.

13 C. K. Chui, *An introduction to wavelet*, Academic Press Inc., San Diego, California (USA), 1992.

14 C. Torrence and G. P. Compo, *Bull. Amer. Meteor. Soc.*, 1998, **79**, 61–78.

15 J. Kirby, *Comput. Geosci.*, 2005, **31**, 846–864.

16 M. Pagliai, G. Cardini, R. Righini and V. Schettino, *J. Chem. Phys.*, 2003, **119**, 6655–6662.

17 M. J. Frisch, G. W. Trucks, H. B. Schlegel, G. E. Scuseria, M. A. Robb, J. R. Cheeseman, J. A. Montgomery Jr., T. Vreven, K. N. Kudin, J. C. Burant, J. M. Millam, S. S. Iyengar, J. Tomasi, V. Barone, B. Mennucci, M. Cossi, G. Scalmani, N. Rega, G. A. Petersson, H. Nakatsuji, M. Hada, M. Ehara, K. Toyota, R. Fukuda, J. Hasegawa, M. Ishida, T. Nakajima, Y. Honda, O. Kitao, H. Nakai, M. Klene, X. Li, J. E. Knox, H. P. Hratchian, J. B. Cross, C. Adamo, J. Jaramillo, R. Gomperts, R. E. Stratmann, O. Yazyev, A. J. Austin, R. Cammi, C. Pomelli, J. W. Ochterski, P. Y. Ayala, K. Morokuma, G. A. Voth, P. Salvador, J. J. Dannenberg, V. G. Zakrzewski, S. Dapprich, A. D. Daniels, M. C. Strain, O. Farkas, D. K. Malick, A. D. Rabuck, K. Raghavachari, J. B. Foresman, J. V. Ortiz, Q. Cui, A. G. Baboul, S. Clifford, J. Cioslowski, B. B. Stefanov, G. Liu, A. Liashenko, P. Piskorz, I. Komaromi, R. L. Martin, D. J. Fox, T. Keith, M. A. Al-Laham, C. Y. Peng, A. Nanayakkara, M. Challacombe, P. M. W. Gill, B. Johnson, W. Chen, M. W. Wong, C. Gonzalez, and J. A. Pople, *Gaussian 03, Revision C.02*, Gaussian, Inc., Wallingford CT, 2004.